Advanced Composite Materials
Publication details, including instructions for authors and subscription information:
http://www.tandfonline.com/loi/tacm20

Fracture behaviour of multi-holed C/C composites

Lars Denk , Hiroshi Hatta , Stoshi Somiya & Misawa Hiroaki

Version of record first published: 02 Apr 2012.

To cite this article: Lars Denk , Hiroshi Hatta , Stoshi Somiya & Misawa Hiroaki (2003): Fracture behaviour of multi-holed C/C composites , Advanced Composite Materials, 12:2-3, 107-122

To link to this article: http://dx.doi.org/10.1163/156855103772658506

Adv. Composite Mater., Vol. 12, No. 2-3, pp. 107–122 (2003)

Also available online - www.vsppub.com

Fracture behaviour of multi-holed C/C composites

LARS DENK [1], HIROSHI HATTA [2,*], STOSHI SOMIYA [1]
and MISAWA HIROAKI [3]

[1] *Keio University, 3-14-1 Hiyoshi, Kohoku-ku, Yokohama, Kanagawa, 233-8522, Japan*
[2] *The Institute of Space and Astronautical Science, 3-1-1 Yoshinodai, Sagamihara, 229-8510, Japan*
[3] *Kanagawa Institute of Technology, 1030 Oginochou, Atugi, 243-0292, Japan*

Received 25 June 2002; accepted 15 January 2003

Abstract—In our previous experiments, the tensile net fracture stress of double-edge-notched carbon–carbon composite (C/C) specimens has been in some cases much higher than that of smooth specimens. To optimally utilize this phenomenon, the tensile fracture behaviour of multi-holed C/Cs with cross-ply lamination was examined. Multi-holed specimens with different numbers of holes and different distances between the holes were prepared and tensile fracture tests were conducted. FEM calculations were performed in order to study the stress distributions during the tensile tests. Higher tensile strength than that of smooth specimens was obtained in an optimal case on the basis of averaged net stress. The strength dependency on the specimen geometry could be explained mainly by the load sharing effect among the ligaments.

Keywords: Carbon/carbon composite; multi-holed specimen; stress concentration; fracture criterion.

1. INTRODUCTION

In our recent papers [1, 2], we have discussed the notch sensitive/insensitive behaviour of carbon–carbon (C/C) composites using double-edge-notched (DEN) specimens. In these tests, we observed anomalous fracture behaviour when the specimen width was narrow, as shown in Fig. 1. This figure was obtained by fixing the ratio of the notch length, a, and the specimen width, W, to $2a/W = 0.5$, and by systematically changing W. When a is small, the net fracture stress $\sigma_{f,net}$ of the notched specimens was much higher than that of smooth specimens, σ_0, as shown by the hatched region. In ordinary materials, this behaviour might be difficult to understand. However, in the case of C/C composites, high strength can be explained easily on some occasions. The ultimate tensile strain of C/C composites (about 0.2%) is usually much lower than that of the reinforcing carbon

*To whom correspondence should be addressed. E-mail: hatta@pub.isas.ac.jp

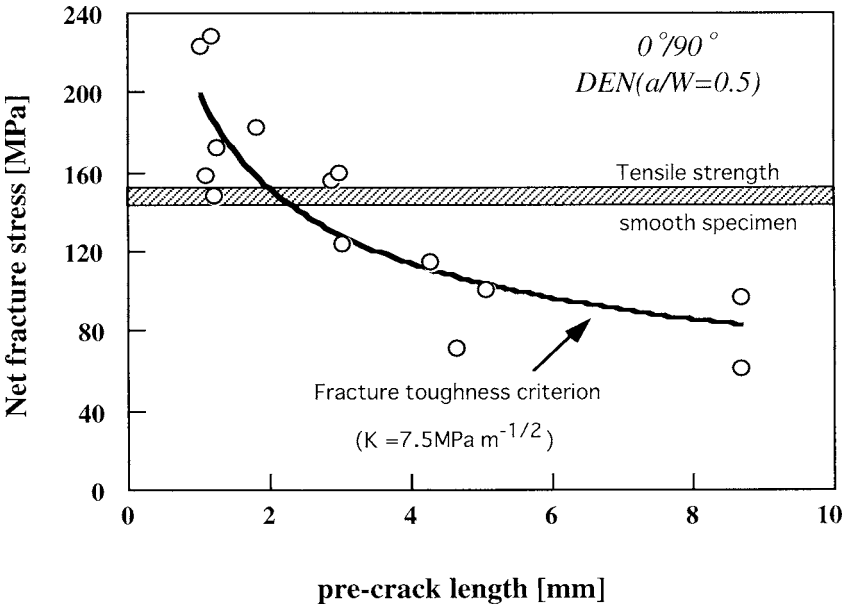

Figure 1. Net fracture stress of double-edge-notched (DEN) C/C composite compared with tensile strength obtained by using smooth specimens (hatched region) and constant toughness line at 7.5 MPa $m^{-1/2}$ (solid line).

fibres (0.65–1.2%). This strain degradation of the C/C composites is believed to be caused by the constraint of the matrix [3]. Hence, if this constraint is relaxed, the ultimate strain of C/C composites can be recovered towards the original higher value of the reinforcing fibres. We considered that the high strength shown in Fig. 1 was produced when the damage zones extending from both notch roots united, thus covering the whole ligament. The damage in the C/C composite in this situation possibly relieved the matrix constraint to the fibres.

The present study was motivated by the above observation and was carried out for two purposes. The first aim was to determine the optimum arrangement of holes in multi-holed specimens under tensile loading. The second was to discuss the origin of this high strength behaviour in relation to the damage zone formation at the notch tips and the weak shear strength characteristics of C/C composites. Since the mechanical response in the damage zone near the holes seems to dictate the notch sensitive/insensitive behavior of C/C composites, it is quite important for the design of actual C/C structures to understand the behavior in the damage zone.

2. EXPERIMENTAL PROCEDURE

2.1. Material

The carbon–carbon composite used in the present study was produced by means of the preformed yarn process [4], and supplied by Across Co. Ltd. It consisted of 16

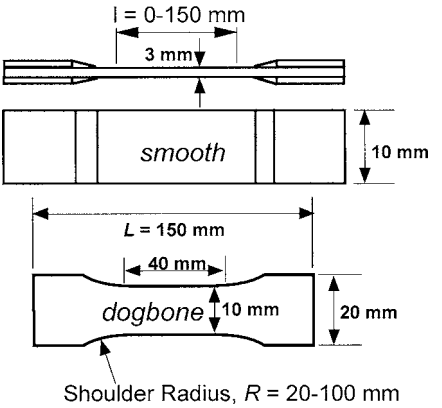

Figure 2. Shapes and dimensions of tensile test specimens.

layers of unidirectionally reinforced laminae arranged into a symmetrical 0°/90° stacking sequence with a total thickness of 3 mm. The reinforcing fibres were polyacrylonitrile (PAN)-based high modulus type TORAYCA®M40. The nominal total volume fraction of the fiber was 0.5.

2.2. Base line data acquisitions

In order to understand the mechanical responses of the C/C and to obtain the necessary data for stress analyses, the tensile and shear properties of the C/C were first obtained. All tests were performed using a screw-driven mechanical testing machine (Shimadzu Co. model AG-5000A) under a crosshead speed of 0.1 mm/min.

2.2.1. Tensile properties. The tensile tests were carried out using coupon and dog-bone-shaped specimens as shown in Fig. 2. In order to determine the optimum geometry, the gage length was varied from 20 mm to 150 mm in the coupon (smooth) specimens, and the shoulder radius was changed in the dog-bone specimens up to 100 mm. Strain gages were attached to both surfaces of a specimen parallel and normal to the loading direction in order to calculate the Young's modulus and Poisson's ratio.

2.2.2. Shear properties. The shear stress–strain relation was measured using the Iosipescu type testing procedure [5]. As shown in Fig. 3, v-notches 6 mm in depth were engraved from both sides of a specimen. Shear strain was determined based on tensile strains measured using gages attached to both surfaces under angles of ±45° with respect to the loading axes.

2.3. Tensile fracture tests of multi-holed specimens

In previous experiments involving single-holed specimens [2], particularly high net fracture stresses were observed when a diameter of hole was 2 mm, and ligament

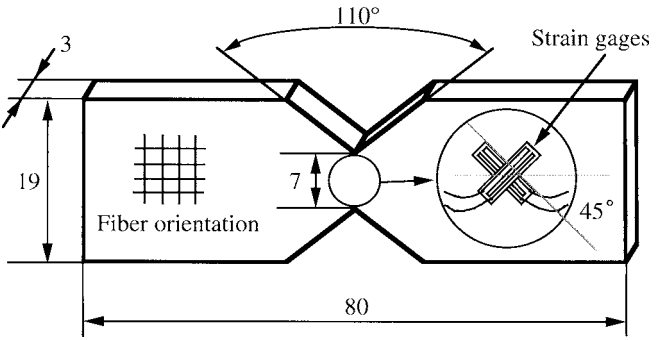

Figure 3. Shape and dimensions of Iosipescu-type specimen.

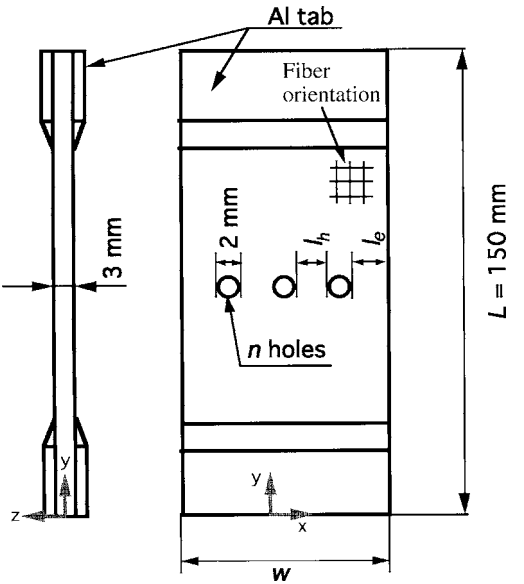

Figure 4. Schematic drawing for multi-holed tensile specimen.

length was short. Thus, similar configurations were also examined in the present experiments as shown in Fig. 4. The geometrical features of the specimens are summarised in Table 1, where l_h, l_e, and n denote the distance between adjacent holes, the distance between the most outer hole and the free edge, and the number of holes, respectively. Hereafter, the series of three figures, $n/l_h/l_e$, and assigned symbols will be used to identify the specimen geometry. During drilling the holes, the surfaces of the specimens were protected by wood layers in order to avoid delamination. Aluminium tabs were attached on both surfaces of the specimens in order to reduce the stress concentrations and to avoid damage caused by gripping. The prepared specimens were then inspected by a microscope, and delaminated specimens were rejected. Three to seven samples in each configuration were fractured.

Table 1.
Specimen geometry

Specimens ($n/l_h/l_e$)	Number of holes n	Hole distance l_h (mm)	Edge distance l_e	Width W (mm)	Symbol
Non-holed	0	—	—	20	⊞
Single-holed	1	—	11	24	×
3/1/1	3	1	1	10	▼
3/4/2	3	4	2	18	◆
3/4/5	3	4	5	24	◇
5/1/1	5	1	1	10	∇
5/2/1	5	2	1	20	▲
5/2/3	5	2	3	24	△
7/1/0.5	7	1	0.5	21	■
7/1/1	7	1	1	22	□
7/1/2	7	1	2	24	○
7/1/4	7	1	4	28	●

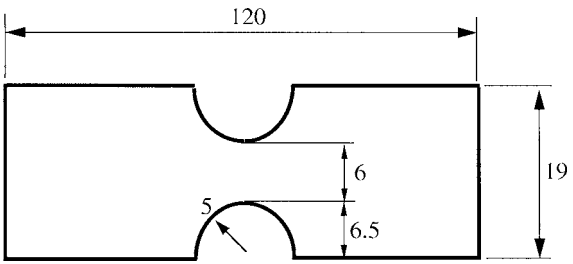

Figure 5. Tensile test specimen used to evaluate the influence of shear damage on tensile strength.

2.4. Tensile fracture tests of unholed specimen after shear predamage

The shear strength of the cross-ply laminated C/C composites is extremely low and the stress–strain relation exhibits strong non-linearity. Thus, even at a low applied load, the shear damage may occur near the stress concentration points of the multi-holed specimens. Accordingly, it is important to identify a damage type as a function of shear stress, especially whether fibre damage accompanies it or not. In order to clarify the initiation point of fibre damage in the shear tests, various loads of shear were preloaded on specimens that were then fractured under tension.

The experimental procedure was as follows. In a calibration step, seven Iosipescu specimens were fractured under shear and the peak shear stress was measured. The results were averaged, and the remaining shear experiments were stopped at up to 200% of the strain at peak stress. In this process, Iosipescu specimens of 120 mm in length were used. The residual tensile strength of all shear-preloaded specimens was then measured. Before the tensile tests, specimens were formed into the shape shown in Fig. 5. This changing configuration was made in order to minimize the effect of stress concentration by the sharp notch of the Iosipescu specimen.

3. FINITE ELEMENT ANALYSES

Finite element calculations of the stress distributions during the tensile tests of the multi-holed specimens were carried out using ABAQUS® with two-dimensional anisotropic models assuming plane stress. The models consisted of between 1200 and 5600 8-node-point isoparametric elements. Tensile and shear stress distributions near the hole tip regions in linear elastic cases were determined using the orthotropic material constants;

$$E_{xx} = E_{yy} = 96.465 \text{ GPa}, \quad \nu_{xy} = 0.026, \quad G_{xy} = 5.4 \text{ Gpa}, \tag{1}$$

where E, ν, and G denote the Young's modulus, Poisson's ratio, and shear modulus, respectively. The material constants were obtained from the above mentioned experiments, and G_{xy} was determined based on the initial slope of the shear stress–strain curve.

In order to evaluate the influence of the extremely low strength and strongly non-linear shear behaviour on the fracture of multi-holed specimens, a non-linear stress–strain analysis was conducted as well. The details of the non-linear calculation procedure will be discussed with the results of shear property tests.

4. RESULTS

4.1. Experimental results

4.1.1. Tensile behaviour. Tensile strength was compared with tensile fracture stresses in multi-holed specimens. Owing to the importance of tensile strength, the influence of specimen geometry on tensile fracture stress was first studied. The tensile fracture stresses obtained using 'dog bone' specimens with a changing shoulder radius, R, and smooth specimens with a changing gage length, l, were compared in Fig. 6. It was concluded from this figure that the tensile fracture stresses obtained using the various specimens were almost identical. Thus, the effects of the gripping and stress concentration from the curvature of the shoulder are negligibly small. The fracture stresses of all the specimens ranged from152 and 206 MPa with an average fracture stress of 186 MPa. This geometry insensitivity in tensile fracture might be caused by the same mechanism as that in the multi-holed specimens discussed below. In spite of the notch insensitivity, all the tensile stress–strain curves were almost linear up to fracture. This tendency is a well known characteristic of C/C composites [2, 6] and differs greatly from that of ceramics matrix composites [7, 8].

4.1.2. Shear test results. C/C composites exhibit a strong non-linear stress–strain curve in shear [7, 9, 10] as typically shown by the solid curve in Fig. 7. Right after the peak shear stress, $\tau_{\max}$, the strain increased rapidly and significantly for a short time, as shown in the lower figure of Fig. 8, where the horizontal axis is

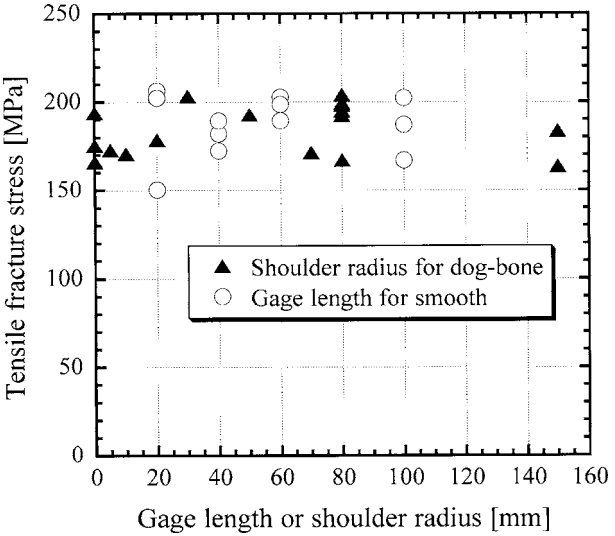

Figure 6. Tensile fracture stress as a function of shoulder angle for dog-bone specimens and gage length for smooth specimens.

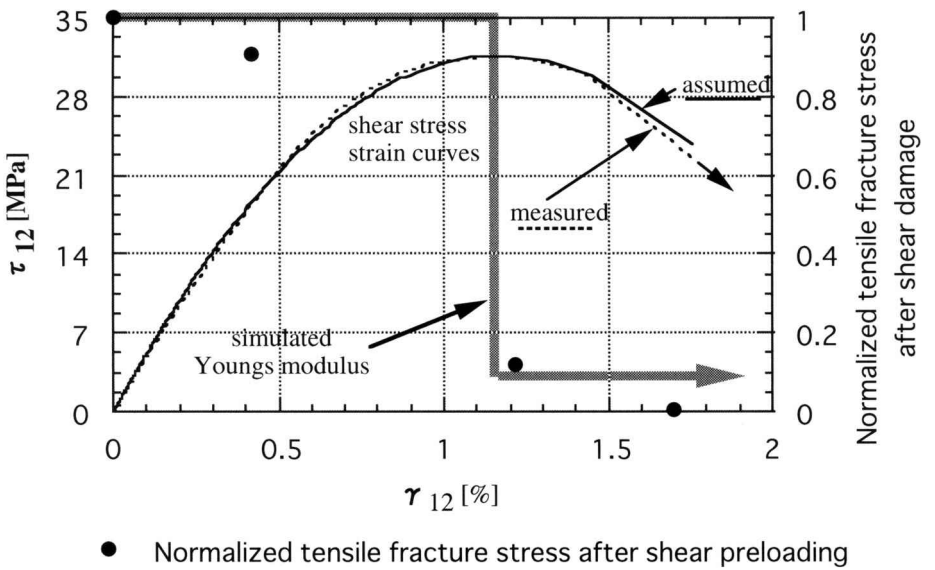

Figure 7. Measured and estimated shear stress-strain curve, simulated Young's modulus as a function of shear strain, and experimentally obtained tensile fracture stress as a function of shear pre-loading.

shear pre-loading time, t. Thus, severe damage was presumed at this point. In order to identify the fiber fracture stress, shear stress was first preloaded on specimens, and the ultimate tensile stress was then measured. The results are depicted in the upper half of Fig. 8, where residual tensile fracture stress (RTS) is plotted against t. As this figure clearly shows, the RTS of shear-preloaded specimen up to τ_{max}, was

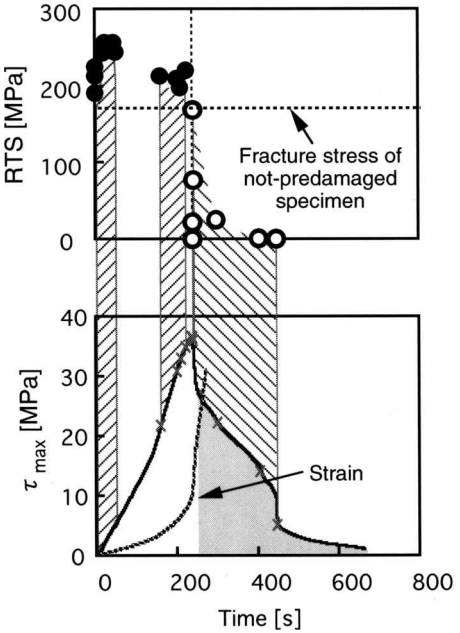

Figure 8. Residual tensile strength (RTS) of C/C after shear damage.

found to be significantly above the RTS of not shear-preloaded specimens as shown by the dotted line in this figure. This result suggests that:

(1) The non-linear shear stress–strain behaviour prior to peak load is not related to fibre failure.

(2) Shear damage eventually produces a higher ultimate tensile strength.

(3) The peak shear stress might coincide with the beginning of fibre failure.

In the finite element calculations, the shear stress–strain curve was modelled by equation (2).

$$\tau_{xy} = 5.4\gamma_{xy} - 2.3\gamma_{xy}^2, \tag{2}$$

where τ_{xy} (GPa) and γ_{xy} (%) represent the shear stress and the shear strain, respectively. The relation between the fitting curve and the actual measured stress–strain data is given in Fig. 7.

On the other hand, even with the shear damage, the tensile stress–strain relation in FEM calculations was assumed to be linear unless shear stress exceeded τ_{max}. However, once it surpassed τ_{max}, the Young's modulus was reduced to one-tenth to simulate the fibre fracture by shear. This reduction rate of Young's modulus was based on the ratio of the average residual strength just after τ_{max} and strength determined by smooth specimens. In the non-linear finite element calculations, the tensile load was increased in 20 steps and the shear modulus G_{xy} changed depending on the local shear strain of the previous step.

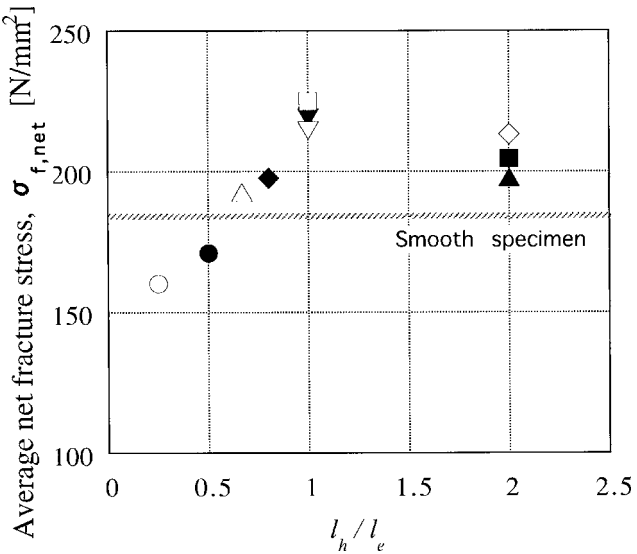

Figure 9. Tensile net fracture stress $\sigma_{f,net}$ of multi-holed specimens.

4.1.3. Tensile test results of multi-holed specimen. The tensile fracture test results of the multi-holed specimens are shown in Fig. 9 in terms of net fracture stresses $\sigma_{f,net} = F_f/A_{net}$, with F_f and A_{net} denoting the fracture load and the net sectional area, respectively. The data is arranged as a function of l_h/l_e. As shown in Fig. 9, $\sigma_{f,net}$ reached a maximum at $l_h/l_e = 1$ and at this point significantly exceeded the strength of the smooth specimens (186 MPa). Hence, the optimum arrangement is located in this area. It follows from this figure that $\sigma_{f,net}$ approximately depends only on the ratio l_h/l_e, which implies that $\sigma_{f,net}$ is insensitive to the hole number n and to the individual ligament length, l_h, or l_e.

4.2. Average tensile stress in the multiholed body

Prior to discussion of the stress distribution in a multiholed body, let us focus on the average stresses in each ligament. It has already been reported that the linear fracture mechanics approach is effective for the discussion of the fracture propagation of C/C used in the present study [1, 2]. This suggests that stress distributions around sharp notches in the C/Cs deviate from those of linear elastic responses only in the vicinity of the notches. Thus, the average stresses were discussed on the basis of orthotropic elastic constants.

For simplicity, let us introduce a model separating the whole specimen (multi-holed body) into single-holed bodies, as shown in Fig. 10. In this model, the edge-sub-elements are modelled by a single-holed body with free boundaries on the one side. In contrast, the center-sub-elements are at first modelled by the infinite body. The infinite body is then reduced into single-holed bodies with straight boundaries on the sides [11]. To these reduced models, the same gross average stress, $\sigma_{gr,ave}$,

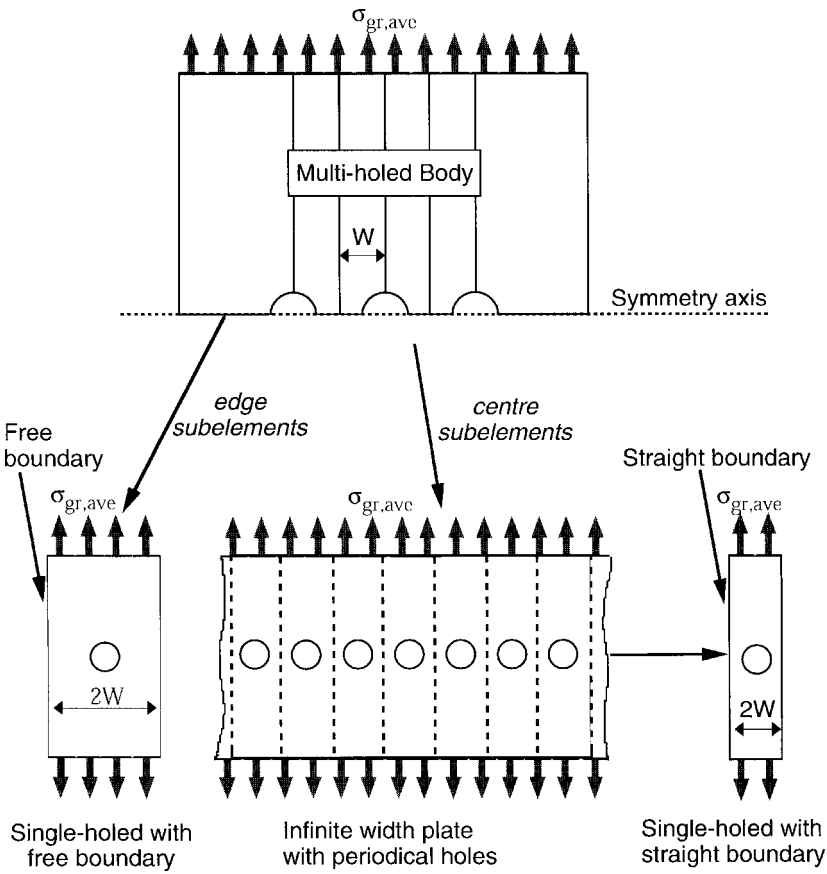

Figure 10. Single-holed bodies used for approximation of stress distributions in a full multi-holed body (actual specimen).

was applied, but the net average stresses, $\sigma_{\text{net,ave}}$s, depend on the ratio of ligament length, w_{net}, and the gross width, w, of the individual sub-elements.

The $\sigma_{\text{net,ave}}$ in the centre and edge ligaments normalized with the $\sigma_{\text{gr,ave}}$ are compared between the full multi-holed and the separated bodies in Fig. 11. It is noted in this figure that the averaged net stresses in both figures are nearly the same. The errors in terms of the average stress were below 5% except for the filled square, 7/1/0.5. Excluding this kind of narrow edge ligament configuration, this hypothesis is quite effective.

In Fig. 12, the stress distributions in the edge and centre portions of the 3/4/2 and 7/1/4 configurations are compared. In this figure, the large dotted and open symbols describe the stress distribution of the complete multi-holed body and of the single-holed approximation, respectively. The distributions are nearly identical. Although the above calculations were made under the assumption of linear elastic response, above results suggest that the model using the separated bodies is effective.

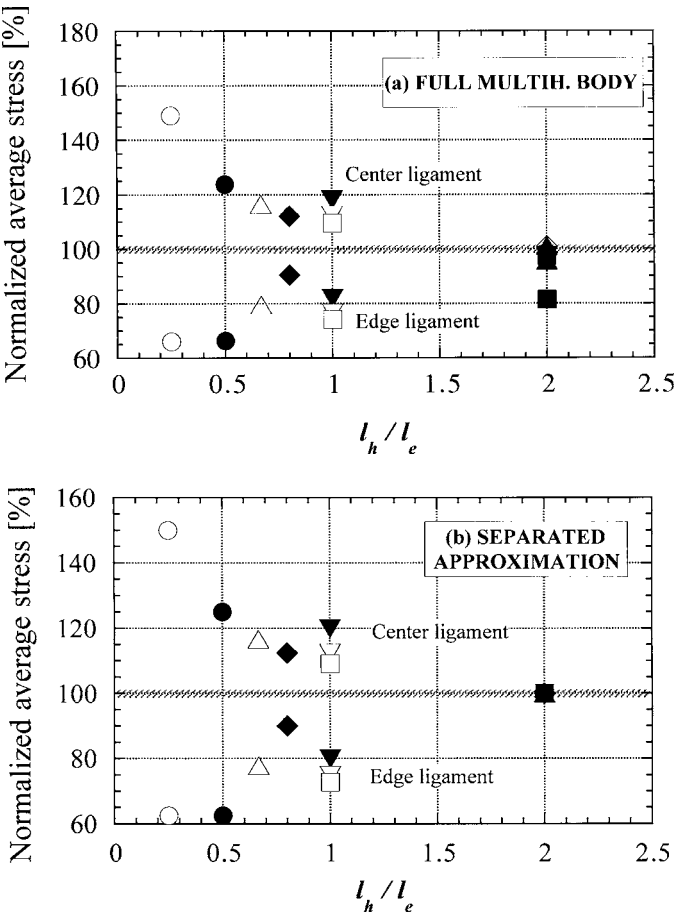

Figure 11. Average stress levels in the centre and edge ligaments as a function of the ratio l_h/l_e for multi-holed specimens (a) and approximated single-holed bodies (b).

4.3. Effect of non-linear shear stress–strain behaviour

Several models have been considered to explain the notch/hole-insensitive behaviour of C/C composites [7, 12–16] among which shear damage-induced stress relaxation [13–15] is one of the most widely discussed. For this case, shear damage propagating parallel to the loading direction was expected to significantly reduce the tensile stress concentrations at notches or holes. The shear damage should be related to the non-linearity of the shear stress–strain curve. Thus, the simulation was carried out using the separated-single-holed model and taking the non-linear stress–strain relation into account. A typical result of the non-linear simulation is illustrated in Fig. 13 for the geometries 3/4/2. The vertical axes in Fig. 13 represent the maximum stress at the outer hole-edge and its stress concentration factor a, defined by maximum stress/net average stress, $\sigma_{\mathrm{net,ave}}$, as a function of $\sigma_{\mathrm{net,ave}}$. In this figure, the tensile stress at the hole-edge increases linearly up to 400 MPa until shear

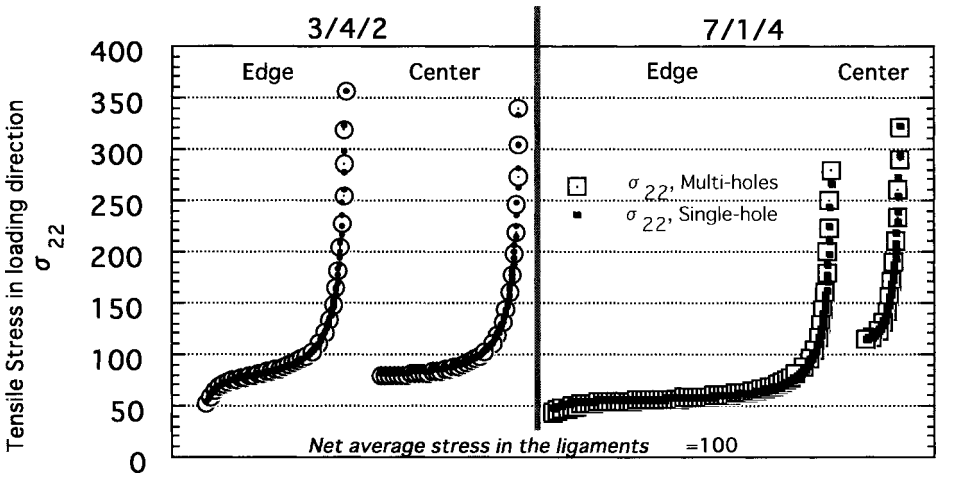

Figure 12. Comparison of tensile stress distributions in multi-holed specimens 7/1/0.5 and 7/1/4 and those in approximated single-holed bodies.

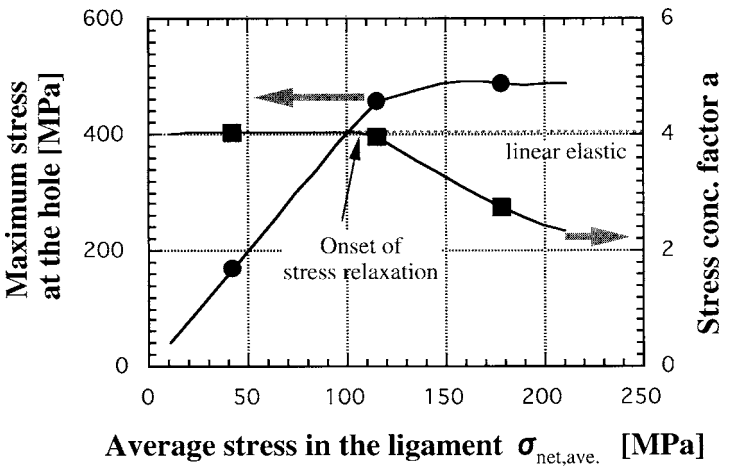

Figure 13. Effect of damage on the stress concentration at the hole tip for the specimen 3/4/2.

damage reduces the stress concentration at the hole. However, the stress relaxation remains too small to explain its fracture in terms of the maximum stress criterion, about twice higher tensile stress than the strength of the present material.

Next, the average net stress $\sigma_{\text{net,ave}}$, of the whole multi-holed 3/4/5 body are compared with those of separated single models of the centre and edge ligaments in Fig. 14. In this figure, in spite of non-linear shear behaviour, the average stresses in the centre and edge ligaments increase almost linearly under the applied load. Thus, it can be concluded that though the shear non-linearity changes the stress concentration at the hole, the average stresses in the individual ligaments is almost identical to those of the linear elastic solution.

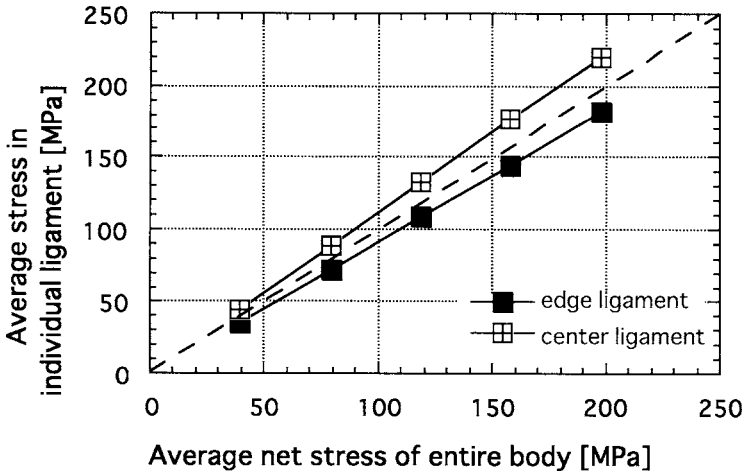

Figure 14. Effect of non-linear shear strain on the average stress in the individual ligament for the specimen 3/4/5.

4.4. Prediction of fracture behaviour

To the authors' knowledge, there are presently no established fracture criteria for brittle matrix composites in regard to rather 'mild' stress concentrations, as for example specimens with holes. Several techniques have been proposed in the past. Among them, three criteria were frequently examined, namely, the linear-elastic fracture mechanics [16], the point stress criterion [2, 17], and the net stress criterion [17]. In the point stress criterion, two parameters, the strength of a smooth specimen, σ_0, and a characteristic distance, d_0, are introduced. Fracture in this criterion is assumed to occur when the stress reaches σ_0 at a distance d_0 from the hole edge. For some ceramic materials, d_0 was shown to be constant [17] and thus this criterion is effective. On the other hand, Kiuchi *et al.* [18] showed for some ceramic matrix composites that the fracture of a notched specimen is simply determined by a constant net sectional stress. We at first examined the applicability of the point stress criterion, and d_0s for multi-holed specimens are plotted in Fig. 15. It can be seen in Fig. 15, the scattering in d_0 is in all cases so large that this criterion is unsuitable in the present case. Then, approach involving the fracture criteria of the critical stress intensity factor K_{Ic} assuming that the hole was replaced by a centre crack with its length equal to the diameter of the holes [16]. This criterion was also confirmed to be unsuitable in the present case. Besides these criteria, maximum stress criterion was examined. This criterion was applied to the highest stress concentration ligaments. However, this criterion was found to be not appropriate.

As shown in Fig. 13, the effect of nonlinear shear deformation at the stress concentration points is not so slight that the average stress criterion becomes another possible candidate. Thus, the ligament of a multi-holed body with the highest net average stress was at first identified. The average stress at fracture, $\sigma_{\text{net-fr}}$, was then calculated. The results are shown in Fig. 16 as a function of l_h/l_e. In this figure, the

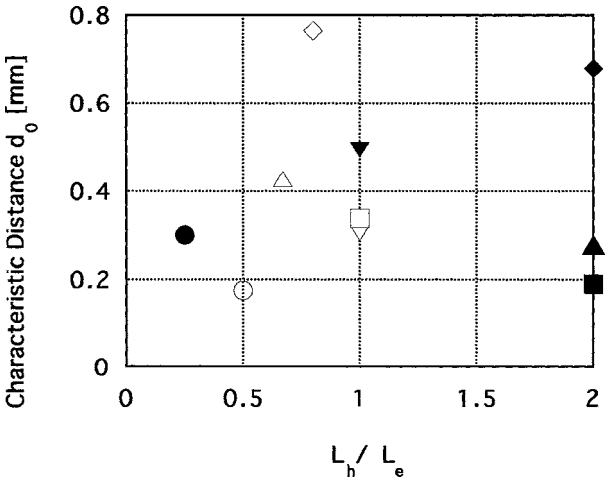

Figure 15. Characteristic distance d_0 of multiholed specimens.

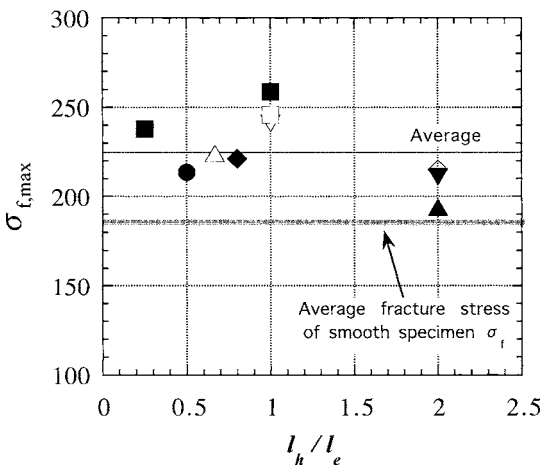

Figure 16. Highest average fracture stress over the ligament σ_{nf} for various multi-holed specimens.

data points gather closely around 225 MPa well above the ultimate tensile strength of smooth specimen, though slightly lower values are resulted for cases of short l_e. Thus, the average fracture stress in the ligament $\sigma_{net\text{-}fr}$ can be successfully used to predict the failure of this type of multi-holed C/C specimen. However, new mechanisms must be introduced to explain the net fracture stress higher than the strength of the material.

5. DISCUSSION

The averaged net fracture stress in the highest stress ligament was in the magnitude of 215 MPa to 260 MPa as shown in Fig. 16. In addition, stress is distributed in

ligaments, and stresses at the hole tips might reach around 400–450 MPa by stress concentration at the hole tips, as shown in Fig. 13. Thus, we must look for a strength enhancing mechanism or other source of stress relaxation which can provide load sustaining capability for such high stresses.

5.1. Strength enhancement

Recently, low interfacial strength was reported to induce high tensile fracture stress and high ultimate elongation in C/C composites [6, 19]. In addition, Fig. 8 showed that when the shear damage is slight, the specimens in the experiment yielded about 1.5 times higher tensile fracture stress than that of a specimen without shear damage. Thus, the strength enhancement in Fig. 16 was speculated to be caused by damage to the interface between the fiber and matrix. However, in the present multi-holed cases, shear cannot provide such damage, since, at the most critical region of the hole tip, shear stress must vanish becase of the symmetrical stress distribution with respect to geometrical symmetric lines. Accordingly, other mechanisms than shear damage should be considered. Cook and Gordon [20] demonstrated that a tensile stress normal to loading direction appears just in front of a crack tip, and this stress causes fibre–matrix debonding if the interfacial strength is low. By this stress, the fibres can be released from the constraint of the matrix as in the case of shear damage. Thus, we can expect that higher loads can be carried in the vicinity of the notch tip of C/C composites.

5.2. Stress relaxation

The described strength enhancing mechanism explained the 1.5 times high tensile stress at the hole-tip. This contribution is not sufficient to explain the high tensile stress at the hole-tips. As a source other than the interfacial damage, stress relaxation by the Cook and Gordon mechanism [20] should be considered. By this mechanism, splitting parallel to the loading direction is expected. The initial splits followed by shear damage can possibly facilitate further relaxation of the stress concentrations.

6. CONCLUDING REMARKS

The examined multi-holed C/C composite specimens showed a significant dependency of the net fracture stress σ_{net} on the two parameters l_{h} and l_{e}. The highest net fracture stress could be obtained for an intermediate value $l_{\text{h}}/l_{\text{e}} = 1$. For this configuration, the maximum net fracture stresses above the fracture stress of smooth specimens were observed. Traditional mechanisms explain only stress relaxation at hole-tip but fail to explain a fracture stress higher than that of the smooth specimen. Recent results show that the C/C composite strength drastically increases if the fibre–matrix interface strength is low. This mechanism is believed to contribute

to the high strength behaviour in the region near the hole observed in the present study.

Acknowledgement

This research was partly supported by grants in aid for basic science (grant No. 11305047) from The Ministry of Education, Sports, Culture, Science and Technology of Japan.

REFERENCES

1. H. Hatta, Y. Kogo, H. Asano and H. Kawada, *Trans. Jap. Soc. Mech. Eng.* **64** (620), 897–903 (1998).
2. Y. Kogo, H. Hatta, H. Kawada and T. Machida, *J. Compos. Mater.* **32**, 1274–1294 (1998).
3. M. Takabatake, in: *Proc. 8th Symp. High Performance Mater. for Severe Environments*, Tokyo, pp. 297–282 (1997–1999).
4. A. Okura and T. Chou, *Adv. Compos. in Emerging Technologies*, 348–353 (1992).
5. D. F. Adams and D. E. Walrath, *Exper. Mech.* **27** (2), 113–119 (1987).
6. H. Hatta, K. Suzuki, T. Sigei, S. Somiya and Y. Sawada, *Carbon* **39**, 83 (2000).
7. A. G. Evans and F. W. Zok, *J. Mater. Sci.* **29**, 3857–3896 (1994).
8. M. D. Thouless, O. Sbaizero, L. S. Sigl and A. G. Evans, *J. Am. Ceram. Soc.* **72** (4), 525–532 (1989).
9. T. J. Mackin, T. E. Purcell, M. Y. He and A. G. Evans, *J. Am. Ceram. Soc.* **78** (7), 1719–1728 (1995).
10. K. R. Turner, J. S. Speck and A. G. Evans, *J. Am. Ceram. Soc.* **78** (7), 1841–1848 (1995).
11. G. N. Savin, *Stress Concentration around Holes*. Pergamon Press (1961).
12. G. Bao and Z. Suo, *Appl. Mech. Rev.* **45** (8), 355–366 (1992).
13. B. N. Cox and C. S. Lo, *Acta Metall. Mater.* **40** (7), 1487–1496 (1992).
14. B. N. Cox and D. B. Marshall, *J. Am. Ceram. Soc.* **79** (5), 1181–1188 (1996).
15. F. E. Heredia, S. M. Spearing, T. J. Mackin, M. Y. He and A. G. Evans, *J. Am. Ceram. Soc.* **77** (11), 2817–2827 (1994).
16. V. Kostopolous and P. Pappas, *Mater. Sci. Eng.* **A250**, 320–327 (1998).
17. J. M. Whitney and R. J. Nuismer, *J. Compos. Mater.* **8**, 253–265 (1974).
18. A. Kiuchi, I. Iwata and N. Nakano, in: *Proc. 4th Symp. High Performance Mater. for Severe Environments*, Tokyo, pp. 37–45 (1993).
19. B. Trouvat, X. Bourrat and R. Naslain, Extended abstracts, in: *23rd Biennial Conf. on Carbon*, Strasbourg, France, pp. 536–537. American Carbon Society (1997).
20. J. Cook and J. E. Gordon, *Proc. Roy. Soc. Lond.* **282** (139), 508–520 (1964).